

## Gigahertz single-electron pumping in silicon with an accuracy better than 9.2 parts in 107

Gento Yamahata, Stephen P. Giblin, Masaya Kataoka, Takeshi Karasawa, and Akira Fujiwara

Citation: [Applied Physics Letters](#) **109**, 013101 (2016); doi: 10.1063/1.4953872

View online: <http://dx.doi.org/10.1063/1.4953872>

View Table of Contents: <http://scitation.aip.org/content/aip/journal/apl/109/1?ver=pdfcov>

Published by the [AIP Publishing](#)

---

### Articles you may be interested in

[High-resolution error detection in the capture process of a single-electron pump](#)

*Appl. Phys. Lett.* **108**, 023502 (2016); 10.1063/1.4939250

[Single-electron pumping from a quantum dot into an electrode](#)

*Appl. Phys. Lett.* **96**, 102105 (2010); 10.1063/1.3319497

[Heating in single-electron pumps driven by surface acoustic waves](#)

*Appl. Phys. Lett.* **88**, 202113 (2006); 10.1063/1.2205169

[Room-temperature single-electron effects in silicon nanocrystal memories](#)

*Appl. Phys. Lett.* **87**, 182106 (2005); 10.1063/1.2123377

[Contribution of the metal/SiO<sub>2</sub> interface potential to photoinduced switching in molecular single-electron tunneling junctions](#)

*J. Appl. Phys.* **97**, 073513 (2005); 10.1063/1.1862319

---

The advertisement features a photograph of the Lake Shore Model 372 cryogenic temperature controller, a white rectangular device with a digital display and control buttons. The display shows '96.837'. To the right, a detailed view of a cryogenic system's internal components, including gold-colored wiring and a blue cylindrical chamber, is shown against a blue background. The text 'Precise temperature control for cryogenic research' is prominently displayed in white, with 'Model 372' in orange below it. The Lake Shore CRYOTRONICS logo is in the top right corner.

# Gigahertz single-electron pumping in silicon with an accuracy better than 9.2 parts in $10^7$

Gento Yamahata,<sup>1,a)</sup> Stephen P. Giblin,<sup>2</sup> Masaya Kataoka,<sup>2</sup> Takeshi Karasawa,<sup>1</sup> and Akira Fujiwara<sup>1</sup>

<sup>1</sup>NTT Basic Research Laboratories, NTT Corporation, 3-1 Morinosato Wakamiya, Atsugi, Kanagawa 243-0198, Japan

<sup>2</sup>National Physical Laboratory, Hampton Road, Teddington, Middlesex TW11 0LW, United Kingdom

(Received 31 March 2016; accepted 1 June 2016; published online 5 July 2016)

High-speed and high-accuracy pumping of a single electron is crucial for realizing an accurate current source, which is a promising candidate for a quantum current standard. Here, using a high-accuracy measurement system traceable to primary standards, we evaluate the accuracy of a Si tunable-barrier single-electron pump driven by a single sinusoidal signal. The pump operates at frequencies up to 6.5 GHz, producing a current of more than 1 nA. At 1 GHz, the current plateau with a level of about 160 pA is found to be accurate to better than 0.92 ppm (parts per million), which is a record value for 1-GHz operation. At 2 GHz, the current plateau offset from  $1ef$  ( $\sim 320$  pA) by 20 ppm is observed. The current quantization accuracy is improved by applying a magnetic field of 14 T, and we observe a current level of  $1ef$  with an accuracy of a few ppm. The presented gigahertz single-electron pumping with a high accuracy is an important step towards a metrological current standard. *Published by AIP Publishing.* [<http://dx.doi.org/10.1063/1.4953872>]

A single electron (SE) can be accurately transferred using a clock-controlled SE pump, which is expected to be used for SE logic circuits,<sup>1</sup> quantum current standards,<sup>2</sup> single-photon sources,<sup>3,4</sup> and electron quantum-optics experiments.<sup>5–7</sup> In particular, a recent proposal to redefine the SI ampere by fixing the elementary charge  $e$  to an exact value<sup>8</sup> has accelerated research on an SE-pumping-based current standard. An electric current  $ef$ , where  $f$  is the input clock frequency, generated by an SE pump could directly realize the SI ampere. In addition, a current standard is an important building block for performing quantum metrology triangle experiments,<sup>9</sup> in which consistency of fundamental physical constants can be checked using the Josephson effect, quantum Hall effect, and SE pumping. In order to realize a practical current standard, it is necessary to achieve high-frequency operation, which results in a high current level; more than 1 nA ( $f > 6.3$  GHz) would be desirable for the closure of the quantum metrology triangle with high precision. More importantly, the SE-pumping accuracy must be sufficiently high; a relative error rate  $\epsilon$  of less than 0.01 ppm (parts per million) is a targeted value.<sup>10</sup>

Many SE-transfer devices have been investigated using normal metals,<sup>11–13</sup> superconducting metals,<sup>14–16</sup> GaAs,<sup>17–23</sup> Si,<sup>24–34</sup> InAs,<sup>35,36</sup> and graphene.<sup>37</sup> One of the most promising devices is a tunable-barrier SE pump,<sup>38</sup> with which gigahertz SE pumping can be achieved<sup>18,27</sup> mainly because the barrier resistance is set low only during the loading and ejection cycles, leading to a low pumping error rate. Recently, three high-accuracy measurements traceable to primary standards have been demonstrated using GaAs tunable-barrier SE pumps: 945-MHz operation with  $\epsilon \leq 1.2$  ppm,<sup>20</sup> 950-MHz operation with  $\epsilon \leq 1.37$  ppm,<sup>39</sup> and 545-MHz operation with  $\epsilon \leq 0.2$  ppm.<sup>40</sup> In contrast, the SE-transfer accuracy of Si devices has been demonstrated to be about 100 ppm using SE

counting<sup>32</sup> and investigated at a 50-ppm level using current measurements.<sup>33</sup> These results were limited by the unoptimized measurement conditions, and they suggest that Si devices are capable of much higher accuracy. In addition, mature Si fabrication techniques enable us to obtain a very small structure, which is important for achieving high accuracy.

In this letter, high-accuracy measurements of a Si tunable-barrier SE pump are reported. We demonstrate 1-GHz pumping with  $\epsilon \leq 0.92$  ppm at a  $1ef$  ( $\sim 160$  pA) current plateau. At 2 GHz, we observe a plateau with a deviation of about 20 ppm from  $1ef$  ( $\sim 320$  pA), but it is improved by applying a magnetic field of 14 T, resulting in an accuracy of about a few ppm around  $1ef$  with a slope of about 0.1 ppm/mV.

Figure 1(a) shows a schematic of the Si SE pump<sup>27</sup> with electrical connections. The device has a double-layer gate structure on an undoped Si wire.<sup>41</sup> We used one device to obtain all data in this letter. The measurement was performed in a helium-3 cryostat without condensation at 1 to 2 K.<sup>41</sup>

Figure 1(b) shows an energy diagram along the Si wire. We perform SE pumping via a small charge island in the Si wire between G1 and G2. A positive DC voltage  $V_{UG}$  is applied to the upper gate to induce electrons in the Si wire. Entrance and exit potential barriers are formed in the Si wire by applying negative DC voltages  $V_{ENT}$  and  $V_{EXIT}$  to G1 and G2, respectively. To pump SEs from the source to drain, the entrance barrier is additionally modulated by a high-frequency sinusoidal signal  $V_{RF}(t)$  using a signal generator (HP 83623B) with frequency  $f$ , which is referenced to a 10-MHz frequency standard.

When the height of the entrance barrier is low, some electrons are loaded into the charge island (loading process). As the entrance barrier rises, the island potential also rises because of a capacitive coupling between G1 and the island. When the potential of the  $n$ th electron is higher than the Fermi level of the source, the electron can escape to the

<sup>a)</sup>yamahata.gento@lab.ntt.co.jp

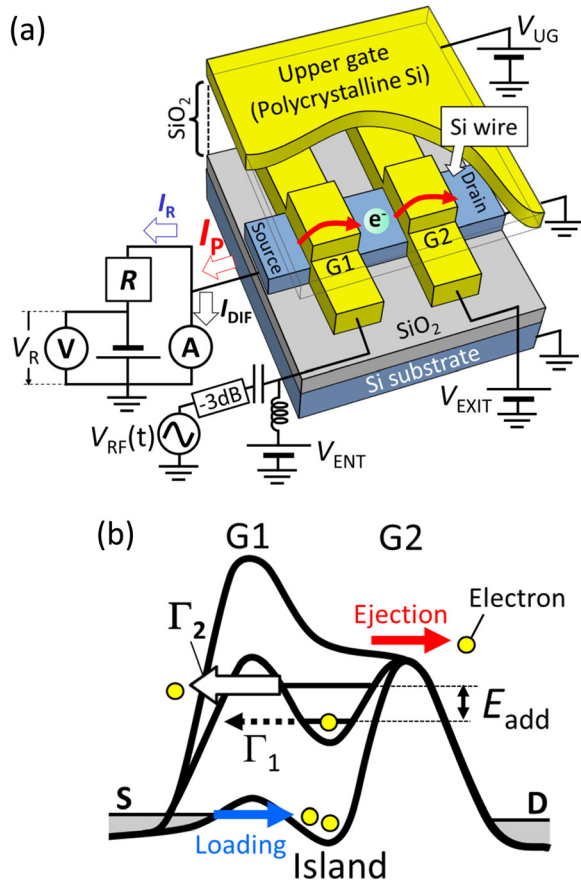


FIG. 1. (a) Schematic of the device with the measurement circuit.  $R$  is the 1-G $\Omega$  standard resistor.  $V_{RF}(t)$  is connected to a 3-dB attenuator and then is connected to  $V_{ENT}$  via a bias tee. The substrate is grounded in all measurements. (b) Energy diagram of the Si wire under G1 and G2. A single electron (SE) loaded from the source is captured by the island and eventually ejected to the drain.

source with rate  $\Gamma_n$ . However, when  $\Gamma_n$  is lower than the characteristic speed of the change in  $\Gamma_n$  ( $\Gamma_n \leq |\dot{\Gamma}_n/\Gamma_n|$ ), the  $n$ th electron is captured by the island. Finally, the captured electron is ejected to the drain (ejection process). When the number of pumped electrons is  $n$  per cycle, the pumping current  $I_P$  is equal to  $nef$ . The most important condition for obtaining a high-accuracy  $1ef$  plateau is  $\Gamma_2 \gg \Gamma_1$ ; a useful parameter is  $\delta \equiv \ln(\Gamma_2/\Gamma_1)$ , which determines a lower bound of the pumping error rate.<sup>42</sup>  $\delta$  more than about 21 is necessary for the operation with an error rate less than  $10^{-8}$ . In the case of a parabolic entrance barrier at a sufficiently low temperature (tunneling regime),  $\delta$  depends on electron addition energy  $E_{add}$  indicated in Fig. 1(b), the curvature of the entrance barrier, and the effective mass of an electron.<sup>32</sup>

To accurately measure  $I_P$ , we use a measurement setup similar to that described in Ref. 20. We use a reference current  $I_R$  generated by applying a voltage to a 1-G $\Omega$  standard resistor  $R$  calibrated in six measurement steps against the quantum Hall resistance standard. The applied voltage is measured using a voltmeter (HP 3458A) calibrated directly against the Josephson voltage standard [Fig. 1(a)]; the reading of the voltmeter is  $V_R$ . The standard resistor is connected to the SE pump, and we measure the current difference  $I_{DIF}$  between  $I_R$  ( $=V_R/R$ ) and  $I_P$  using a current amplifier (Femto DDP-300) and a voltmeter (Agilent 34420A);  $I_P = I_R + I_{DIF}$ . When

$I_{DIF} \ll I_R$  ( $I_P \sim I_R$ ), the relative systematic (type-B) uncertainty  $U_B$  of the measurement of  $I_P$  is

$$\frac{\Delta(I_P)}{I_P} = \frac{\Delta(I_R + I_{DIF})}{I_R + I_{DIF}} = \frac{\sqrt{[\Delta(I_R)]^2 + [\Delta(I_{DIF})]^2}}{I_R + I_{DIF}} \sim \sqrt{\left[\frac{\Delta(I_R)}{I_R}\right]^2 + \left[\frac{\Delta(I_{DIF})}{I_R}\right]^2}, \quad (1)$$

where  $\Delta(*)$  is a type-B uncertainty of the measurement of  $*$ . The first term of Eq. (1) is the relative type-B uncertainty of the measurement of  $I_R$ ; Table I summarizes the main contributions to the uncertainty budget, and  $\Delta(I_R)/I_R = 0.88$  ppm. In contrast, the second term,  $\Delta(I_{DIF})/I_R$ , is much smaller and less than 0.1 ppm when  $I_R$  is more than three orders of magnitude larger than  $I_{DIF}$  because

$$\frac{\Delta(I_{DIF})}{I_R} = \frac{\Delta(I_{DIF})}{I_{DIF}} \times \frac{I_{DIF}}{I_R} \sim 100 \text{ ppm} \times \frac{I_{DIF}}{I_R}, \quad (2)$$

where  $\Delta(I_{DIF})/I_{DIF} \sim 100$  ppm is the uncertainty due to the current amplifier gain, which is calibrated using the 1-G $\Omega$  standard resistor. Thus, the second term is negligible and  $U_B = 0.88$  ppm. Note that we tune the voltage applied to the 1-G $\Omega$  standard resistor to achieve the condition  $I_{DIF}/I_R < 10^{-3}$ .

First, we measure  $I_P$  without  $I_R$  ( $V_R \sim 0$ ) to investigate how fast the Si pump can operate. Figure 2(a) shows a two-dimensional map of  $I_P$  as a function of  $V_{EXIT}$  and  $V_{ENT}$  at 1 GHz, where the current level of the  $1ef$  plateau is about 160 pA. The boundaries of the current plateaus ( $1ef$ ,  $2ef$ , and  $3ef$ ) in the map are determined by the loading, capture ( $\Gamma_1$ ,  $\Gamma_2$ , and  $\Gamma_3$ ), and ejection processes discussed above, as indicated by the blue, black, and red lines, respectively. This is a typical current map of tunable-barrier pumps.<sup>38</sup>

Figure 2(b) shows  $I_P$  as a function of  $V_{EXIT}$  at 1, 2, and 6.5 GHz. We observe a clear  $1ef$  plateau with a current level of more than 1 nA at 6.5 GHz. We fit these characteristics [red curves in Fig. 2(b)] using a formula based on a non-equilibrium SE capture<sup>42</sup> given by

$$I_P/ef = \sum_{k=1}^2 \exp\left[-\exp\left(-\delta \times \frac{V_{EXIT} - V_k}{V_2 - V_1}\right)\right], \quad (3)$$

where  $V_k$  is the threshold voltage of the  $k$ th current plateau. From the fits,  $\delta$ 's at 1, 2, and 6.5 GHz are extracted to be about 23, 22, and 9, respectively. This indicates that the lower bound of the relative error rate<sup>20,32</sup> is less than 0.01 ppm at 1 and 2 GHz but on the order of 1000 ppm at

TABLE I. Uncertainty budget of the measurement of  $I_R$ . We neglect uncertainties less than 0.1 ppm. The 10-M $\Omega$  resistor was used in the calibration of the 1 G $\Omega$  resistor.

| Contribution                        | Type-B uncertainty (ppm) |
|-------------------------------------|--------------------------|
| 1-G $\Omega$ calibration            | 0.8                      |
| 1-G $\Omega$ drift extrapolation    | 0.3                      |
| 10-M $\Omega$ reference resistor    | 0.1                      |
| Voltmeter calibration               | 0.1                      |
| Voltmeter drift between calibration | 0.15                     |
| Total                               | 0.88                     |

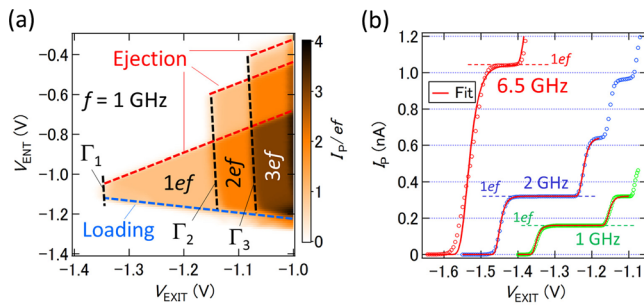


FIG. 2. (a) Pumping current  $I_p$  normalized by  $ef$  as a function of  $V_{\text{EXIT}}$  and  $V_{\text{ENT}}$  at 1 GHz, where  $V_{\text{UG}} = 4.2$  V, the power of  $V_{\text{RF}}(t)$  is 12 dBm, and magnetic field  $B = 0$  T. The blue, black, and red dashed lines correspond to the loading, capture, and ejection processes of the SE pumping. (b)  $I_p$  as a function of  $V_{\text{EXIT}}$ , where  $B = 0$  T. For the 1-GHz data (green circles),  $V_{\text{UG}} = 4.2$  V,  $V_{\text{ENT}} = -1.06$  V, and the power of  $V_{\text{RF}}(t)$  is 12 dBm. For the 2-GHz data (blue circles),  $V_{\text{UG}} = 4.2$  V,  $V_{\text{ENT}} = -1.11$  V, and the power of  $V_{\text{RF}}(t)$  is 13.2 dBm. For the 6.5-GHz data (red circles),  $V_{\text{UG}} = 3$  V,  $V_{\text{ENT}} = -0.6$  V, and the power of  $V_{\text{RF}}(t)$  is 10 dBm. Red curves are theoretical fits to the data.

6.5 GHz. This accuracy degradation with increasing frequency could originate from a decrease in  $E_{\text{add}}$  due to the different potential shape with which the second-last electron escapes to the source<sup>43</sup> or from nonadiabatic excitation.<sup>44</sup> In addition, the fitting curve of the 6.5-GHz data has a deviation against the raw data. The origin of the accuracy degradation and fitting deviation is not yet clear and needs further investigation.

It is worth mentioning that special gate-driving techniques, such as a non-sinusoidal input waveform<sup>20,40</sup> and two phase-shifted sinusoidal waves,<sup>40</sup> are often used in GaAs pumps to observe a clear current plateau at about 1 GHz. The purpose of using these techniques is to reduce the rise rate of the island potential as it crosses the Fermi level and thereby slow down the electron capture process. In contrast, a single sinusoidal input waveform is used in this work. The Si pump tends to have larger  $E_{\text{add}}$  than GaAs pumps,<sup>20,40</sup> which allows accurate pumping for faster potential rise rates and single sinusoidal drive at higher frequencies. This simple operation is suitable for practical applications.

Since we expected high-accuracy operation from the  $\delta$  estimation at 1 and 2 GHz, we performed the high-accuracy measurements using  $I_R$ . In actual measurements, we need to reduce the random (type-A) uncertainty by integrating many data points. To minimize the effect of  $1/f$  noise in the current amplifier at a low frequency and to remove an offset voltage in the current amplifier, we measured  $I_{\text{DIF}}$  while turning on and off  $I_p$  and  $I_R$ .<sup>41</sup> Typical raw data of  $I_R$  and  $I_{\text{DIF}}$  as a function of the number of measurements are shown in Fig. 3(a). After subtracting the off-state data from the on-state ones ( $I_{\text{R}}^{\text{ON}} - I_{\text{R}}^{\text{OFF}}$ ,  $I_{\text{DIF}}^{\text{ON}} - I_{\text{DIF}}^{\text{OFF}}$ ), we average them to extract the mean and the type-A uncertainty of  $I_p$ . Since  $I_{\text{R}}^{\text{ON}} - I_{\text{R}}^{\text{OFF}}$  is about  $10^{-10}$  A and  $I_{\text{DIF}}^{\text{ON}} - I_{\text{DIF}}^{\text{OFF}}$  is less than  $10^{-13}$  A, we neglect the type-B uncertainty of the measurement of  $I_{\text{DIF}}$  as discussed above.

Figure 3(b) shows the deviation of  $I_p$  from  $ef$  as a function of  $V_{\text{EXIT}}$  at 1 GHz, where the deviation is normalized by  $ef$ . The error bar of each individual data point indicates the relative type-A uncertainty. Since the two slopes indicated by black arrows are clearly much steeper than those in the

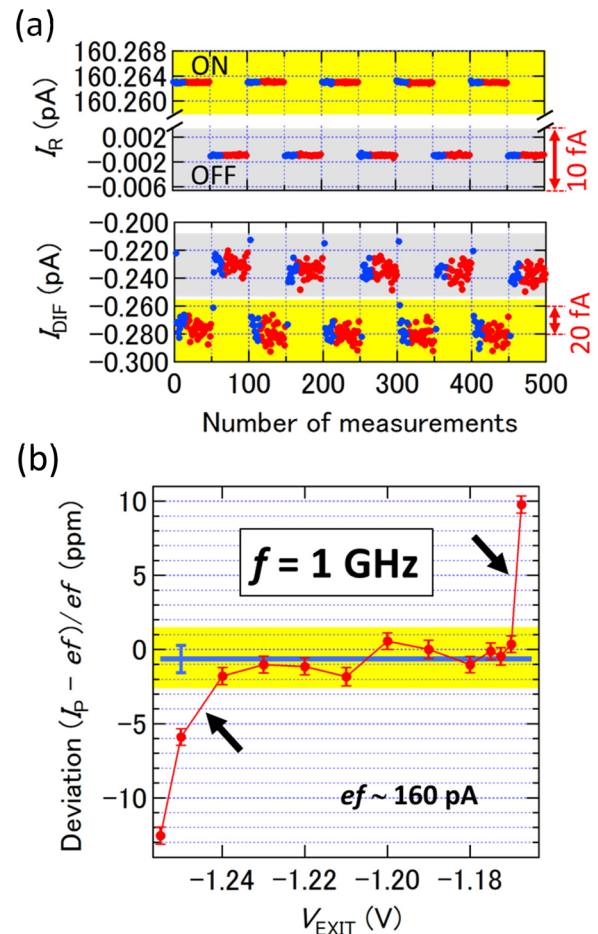


FIG. 3. (a) Typical  $I_R$  and  $I_{\text{DIF}}$  as a function of the number of measurements at 1 GHz, where  $V_{\text{UG}} = 4.2$  V,  $V_{\text{ENT}} = -1.06$  V, the power of  $V_{\text{RF}}(t)$  is 12 dBm, and  $B = 0$ . The yellow and gray regions correspond to the on-state and off-state,<sup>41</sup> respectively.  $I_{\text{DIF}}$  has an offset of about  $-0.2$  pA, which originates from the current amplifier. We ignore blue points and integrate only red points to extract  $I_p$ . Note that the type-A uncertainty is dominated by the measurement of  $I_{\text{DIF}}$ , which is clearly seen from the distribution of the data points (b) Normalized deviation of  $I_p$  from  $ef$  as a function of  $V_{\text{EXIT}}$  at 1 GHz, where  $V_{\text{UG}} = 4.2$  V,  $V_{\text{ENT}} = -1.06$  V, the power of  $V_{\text{RF}}(t)$  is 12 dBm, and  $B = 0$ . The error bar of each data point is the relative type-A uncertainty. The blue line and error bar indicate the mean and total uncertainty of the data in the plateau (yellow region), respectively.

yellow square region, we used the ten data points in the region for the estimation of the total uncertainty  $U_T$ . The scattering of the data points in this region is consistent with a Gaussian distribution due to random noise, but there is a possibility that they exhibit a slope or drift at less than 1-ppm level, which cannot be clearly resolved. However, since the level of the possible slope or drift is small, we consider that these ten data points form a plateau. Then, we average the ten points and obtain the mean current of  $(-0.64 \pm 0.92)$  ppm, shown on the plot at the horizontal blue line and error bar. Here,  $U_T$  of 0.92 ppm includes a 0.27-ppm type-A contribution.<sup>41</sup> This data demonstrate the first high-accuracy operation of a silicon SE pump (the relative pumping error rate of less than 0.92 ppm) and is also the most accurate SE pumping reported to date at 1 GHz. Note that it is comparable to the uncertainty of the metrological triangle experiment using the electron counting capacitance standard.<sup>45</sup>

We also performed high-accuracy measurements at 2 GHz. In this case, we observed a current plateau as a function

of  $V_{\text{EXIT}}$  with a relative deviation of about 20 ppm from  $1ef$  (green curve in Fig. 4). In GaAs pumps, applying a magnetic field has been shown to improve the pumping accuracy.<sup>46</sup> This is attributed to the change in the effective barrier shape due to magnetic confinement. In order to investigate the effect of applying a magnetic field in Si pumps, we extract  $\delta$  of the  $1ef$  plateau at 2 GHz from a fit similar to that shown in Fig. 2(b) with changing magnetic field. As shown in the inset in Fig. 4,  $\delta$  increases with increasing magnetic field. Note that the corresponding reduced- $\chi^2$  values are almost constant, indicating that the fits for extracting  $\delta$  do not degrade with applied magnetic fields. This enhancement indicates a change in  $E_{\text{add}}$  or in the effective barrier shape. Both effects can be attributed to magnetic confinement of the electron wave function in the island. Note that the effect of the magnetic field is weaker than in GaAs pumps, which could be because the island size in the Si pump is smaller. When we apply a magnetic field of 14 T, the plateau shifts closer to  $1ef$  (red curve in Fig. 4). Similar to the 1-GHz data, the slopes are gentler in the yellow square region than outside it. From the nine data points in the yellow square region, the mean and  $U_T$  are estimated to be  $(-0.67 \pm 0.97)$  ppm. However, there is still a slope of about 0.1 ppm/mV indicated by a linear fit (blue line) in the yellow square region. Nevertheless, it is important to note that a current level of about 320 pA can be generated with an accuracy of a few ppm when we set  $V_{\text{EXIT}}$  between  $-1.30$  and  $-1.26$  V.

The origin of the non-quantized current plateau in the 2-GHz pumping and of the improvement of the accuracy by applying the magnetic field is not clear, but we speculate about two possibilities. One is a potential fluctuation. As discussed above, the potential curvature of the entrance barrier is one of the critical points that determine the accuracy.<sup>32</sup>

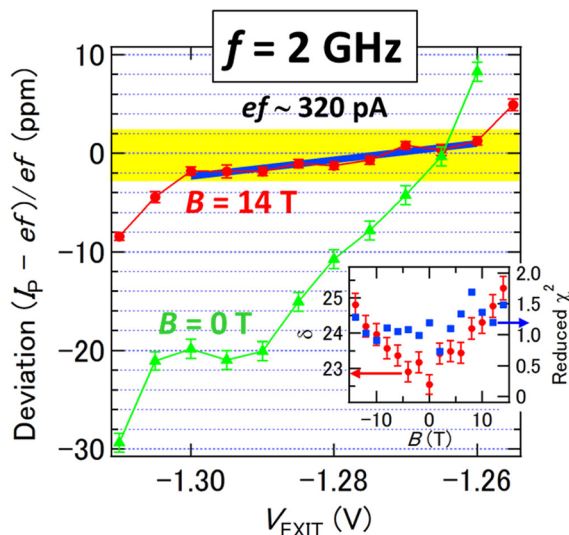


FIG. 4. Normalized deviation of  $I_p$  from  $ef$  as a function of  $V_{\text{EXIT}}$  at  $f = 2$  GHz. For the green curve,  $V_{\text{UG}} = 4.2$  V,  $V_{\text{ENT}} = -1.11$  V, the power of  $V_{\text{RF}}(t)$  is 13 dBm, and  $B = 0$  T. For the red curve,  $V_{\text{UG}} = 4.2$  V,  $V_{\text{ENT}} = -1.11$  V, the power of  $V_{\text{RF}}(t)$  is 12.2 dBm, and  $B = 14$  T. The error bar of each data point is the relative type-A uncertainty. The blue line is a linear fit with a slope of about 0.1 ppm/mV. Note that we did not observe a large change in accuracy when the power of  $V_{\text{RF}}(t)$  was changed. Inset:  $\delta$  (left axis) and reduced- $\chi^2$  values (right axis) extracted from a fit to 2-GHz pumping data, in which we set a typical error bar (1%) for all data points, similar to that shown in Fig. 2(b) as a function of  $B$ .

When we change operating parameters such as  $f$  and  $V_{\text{EXIT}}$ , the capture condition during the rise of the entrance barrier should change. If there is a potential fluctuation in the entrance barrier, the potential curvature experienced by an SE at the capture condition would be different when we change the operating parameters. This could result in the non-quantized current plateau of the 2-GHz operation. In this case, the magnetic field should be another parameter that changes the capture condition because of the magnetic confinement of the electron wave function, which might cause the observed improvement of the accuracy. The other possibility is a nonadiabatic excitation effect.<sup>44</sup> When the speed of change in the island shape is fast during the rise of the entrance barrier, an SE loaded at the ground state of the island can be nonadiabatically excited to the excited state. Then, an SE that populates the excited state easily spills out to the source, leading to an error in the SE pumping. This effect can be enhanced with increasing speed of the change in the island shape. Since we do not observe the 20-ppm-level plateau at less than 1 GHz, this feature could be related to nonadiabatic excitation. In addition, the effect can be suppressed by increasing the magnetic field.<sup>46</sup> This would be qualitatively consistent with our observation. In future work, we need further study to elucidate this point.

In conclusion, we have demonstrated 1-GHz SE pumping with a record relative error rate of less than 0.92 ppm in a Si tunable-barrier pump with a single sinusoidal driving signal. In the case of 2-GHz pumping, applying a magnetic field improves the accuracy, and the current of around  $1ef$  has an accuracy of about a few ppm with a slope of about 0.1 ppm/mV, which could be due to potential fluctuation or nonadiabatic excitation. This demonstration of the high-speed and high-accuracy pumping will open the door to quantum current standards based on Si tunable-barrier SE pumps. In addition, our result, along with precision measurements on GaAs pumps,<sup>20,39,40</sup> implies that accurate pumping in a tunable-barrier pump is universal at the ppm level. For decreasing the type-B uncertainty to a value below 0.88 ppm, one possibility is to use higher-accuracy measurement systems such as an ultrastable low-noise current amplifier<sup>40</sup> or a cryogenic current comparator.<sup>47</sup> SE counting measurements<sup>32,48</sup> can also yield precision information about the pumping characteristics.

We thank H. Tanaka, J. D. Fletcher, and T. J. B. M. Janssen for useful discussions. This work was partly supported by the UK Department for Business, Innovation, and Skills.

<sup>1</sup>K. Nishiguchi, A. Fujiwara, Y. Ono, H. Inokawa, and Y. Takahashi, *Appl. Phys. Lett.* **88**, 183101 (2006).

<sup>2</sup>J. P. Pekola, O.-P. Saira, V. F. Maisi, A. Kemppinen, M. Möttönen, Y. A. Pashkin, and D. V. Averin, *Rev. Mod. Phys.* **85**, 1421 (2013).

<sup>3</sup>J. Kim, O. Benson, H. Kan, and Y. Yamamoto, *Nature* **397**, 500 (1999).

<sup>4</sup>O. D. Couto, Jr., S. Lazić, F. Iikawa, J. A. H. Stotz, U. Jahn, R. Hey, and P. V. Santos, *Nat. Photonics* **3**, 645 (2009).

<sup>5</sup>E. Bocquillon, F. D. Parmentier, C. Grenier, J.-M. Berroir, P. Degiovanni, D. C. Glatthli, B. Plaçaïs, A. Cavanna, Y. Jin, and G. Fève, *Phys. Rev. Lett.* **108**, 196803 (2012).

<sup>6</sup>J. D. Fletcher, P. See, H. Howe, M. Pepper, S. P. Giblin, J. P. Griffiths, G. A. C. Jones, I. Farrer, D. A. Ritchie, T. J. B. M. Janssen, and M. Kataoka, *Phys. Rev. Lett.* **111**, 216807 (2013).

- <sup>7</sup>N. Ubbelohde, F. Hohls, V. Kashcheyevs, T. Wagner, L. Fricke, B. Kästner, K. Pierz, H. W. Schumacher, and R. J. Haug, *Nat. Nanotechnol.* **10**, 46 (2015).
- <sup>8</sup>I. M. Mills, P. J. Mohr, T. J. Quinn, B. N. Taylor, and E. R. Williams, *Metrologia* **43**, 227 (2006).
- <sup>9</sup>F. Piquemal and G. Genevès, *Metrologia* **37**, 207 (2000).
- <sup>10</sup>N. Feltin and F. Piquemal, *Eur. Phys. J. Special Topics* **172**, 267 (2009).
- <sup>11</sup>L. J. Geerligs, V. F. Anderegg, P. A. M. Holweg, J. E. Mooij, H. Pothier, D. Esteve, C. Urbina, and M. H. Devoret, *Phys. Rev. Lett.* **64**, 2691 (1990).
- <sup>12</sup>H. Pothier, P. Lafarge, C. Urbina, D. Esteve, and M. H. Devoret, *Europhys. Lett.* **17**, 249 (1992).
- <sup>13</sup>M. W. Keller, J. M. Martinis, N. M. Zimmerman, and A. H. Steinbach, *Appl. Phys. Lett.* **69**, 1804 (1996).
- <sup>14</sup>J. P. Pekola, J. J. Vartiainen, M. Möttönen, O.-P. Saira, M. Meschke, and D. V. Averin, *Nat. Phys.* **4**, 120 (2008).
- <sup>15</sup>V. F. Maisi, Y. A. Pashkin, S. Kafanov, J.-S. Tsai, and J. P. Pekola, *New J. Phys.* **11**, 113057 (2009).
- <sup>16</sup>S. Nakamura, Y. A. Pashkin, J. S. Tsai, and N. Kaneko, *IEEE Trans. Instrum. Meas.* **64**, 1696 (2015).
- <sup>17</sup>L. P. Kouwenhoven, A. T. Johnson, N. C. van der Vaart, C. J. P. M. Harmans, and C. T. Foxon, *Phys. Rev. Lett.* **67**, 1626 (1991).
- <sup>18</sup>M. D. Blumenthal, B. Kaestner, L. Li, S. Giblin, T. J. B. M. Janssen, M. Pepper, D. Anderson, G. Jones, and D. A. Ritchie, *Nat. Phys.* **3**, 343 (2007).
- <sup>19</sup>B. Kaestner, V. Kashcheyevs, S. Amakawa, M. D. Blumenthal, L. Li, T. J. B. M. Janssen, G. Hein, K. Pierz, T. Weimann, U. Siegner, and H. W. Schumacher, *Phys. Rev. B* **77**, 153301 (2008).
- <sup>20</sup>S. P. Giblin, M. Kataoka, J. D. Fletcher, P. See, T. J. B. M. Janssen, J. P. Griffiths, G. A. C. Jones, I. Farrer, and D. A. Ritchie, *Nat. Commun.* **3**, 930 (2012).
- <sup>21</sup>L. Fricke, M. Wulf, B. Kaestner, V. Kashcheyevs, J. Timoshenko, P. Nazarov, F. Hohls, P. Mirovsky, B. Mackrodt, R. Dolata, T. Weimann, K. Pierz, and H. W. Schumacher, *Phys. Rev. Lett.* **110**, 126803 (2013).
- <sup>22</sup>L. Fricke, M. Wulf, B. Kaestner, F. Hohls, P. Mirovsky, B. Mackrodt, R. Dolata, T. Weimann, K. Pierz, U. Siegner, and H. W. Schumacher, *Phys. Rev. Lett.* **112**, 226803 (2014).
- <sup>23</sup>M. Seo, Y.-H. Ahn, Y. Oh, Y. Chung, S. Ryu, H.-S. Sim, I.-H. Lee, M.-H. Bae, and N. Kim, *Phys. Rev. B* **90**, 085307 (2014).
- <sup>24</sup>Y. Ono and Y. Takahashi, *Appl. Phys. Lett.* **82**, 1221 (2003).
- <sup>25</sup>A. Fujiwara, N. M. Zimmerman, Y. Ono, and Y. Takahashi, *Appl. Phys. Lett.* **84**, 1323 (2004).
- <sup>26</sup>D. Moraru, Y. Ono, H. Inokawa, and M. Tabe, *Phys. Rev. B* **76**, 075332 (2007).
- <sup>27</sup>A. Fujiwara, K. Nishiguchi, and Y. Ono, *Appl. Phys. Lett.* **92**, 042102 (2008).
- <sup>28</sup>G. Yamahata, K. Nishiguchi, and A. Fujiwara, *Appl. Phys. Lett.* **98**, 222104 (2011).
- <sup>29</sup>G. P. Lansbergen, Y. Ono, and A. Fujiwara, *Nano Lett.* **12**, 763 (2012).
- <sup>30</sup>X. Jehl, B. Voisin, T. Charron, P. Clapera, S. Ray, B. Roche, M. Sanquer, S. Djordjevic, L. Devoille, R. Wacquez, and M. Vinet, *Phys. Rev. X* **3**, 021012 (2013).
- <sup>31</sup>B. Roche, R.-P. Riwar, B. Voisin, E. Dupont-Ferrier, R. Wacquez, M. Vinet, M. Sanquer, J. Splettstoesser, and X. Jehl, *Nat. Commun.* **4**, 1581 (2013).
- <sup>32</sup>G. Yamahata, K. Nishiguchi, and A. Fujiwara, *Phys. Rev. B* **89**, 165302 (2014); G. Yamahata, K. Nishiguchi, and A. Fujiwara, *ibid.* **90**, 039908(E) (2014).
- <sup>33</sup>A. Rossi, T. Tanttu, K. Y. Tan, I. Iisakka, R. Zhao, K. W. Chan, G. C. Tettamanzi, S. Rogge, A. S. Dzurak, and M. Möttönen, *Nano Lett.* **14**, 3405 (2014).
- <sup>34</sup>G. Yamahata, K. Nishiguchi, and A. Fujiwara, *Nat. Commun.* **5**, 5038 (2014).
- <sup>35</sup>A. Fuhrer, C. Fasth, and L. Samuelson, *Appl. Phys. Lett.* **91**, 052109 (2007).
- <sup>36</sup>S. d'Hollosy, M. Jung, A. Baumgartner, V. A. Guzenko, M. H. Madsen, J. Nygård, and C. Schönenberger, *Nano Lett.* **15**, 4585 (2015).
- <sup>37</sup>M.-R. Connolly, K. L. Chiu, S. P. Giblin, M. Kataoka, J. D. Fletcher, C. Chua, J. P. Griffiths, G. A. C. Jones, V. I. Fal'ko, C. G. Smith, and T. J. B. M. Janssen, *Nat. Nanotechnol.* **8**, 417 (2013).
- <sup>38</sup>B. Kaestner and V. Kashcheyevs, *Rep. Prog. Phys.* **78**, 103901 (2015).
- <sup>39</sup>M.-H. Bae, Y.-H. Ahn, M. Seo, Y. Chung, J. D. Fletcher, S. P. Giblin, M. Kataoka, and N. Kim, *Metrologia* **52**, 195 (2015).
- <sup>40</sup>F. Stein, D. Drung, L. Fricke, H. Scherer, F. Hohls, C. Leicht, M. Götz, C. Krause, R. Behr, E. Pesel, K. Pierz, U. Siegner, F. J. Ahlers, and H. W. Schumacher, *Appl. Phys. Lett.* **107**, 103501 (2015).
- <sup>41</sup>See supplementary information at <http://dx.doi.org/10.1063/1.4953872> for the device fabrication process, the measurement temperatures, rough estimation of  $E_{\text{add}}$ , the detail about the on-off measurement, and the type-A uncertainty.
- <sup>42</sup>V. Kashcheyevs and B. Kaestner, *Phys. Rev. Lett.* **104**, 186805 (2010).
- <sup>43</sup>G. Yamahata, T. Karasawa, and A. Fujiwara, *Appl. Phys. Lett.* **106**, 023112 (2015).
- <sup>44</sup>M. Kataoka, J. D. Fletcher, P. See, S. P. Giblin, T. J. B. M. Janssen, J. P. Griffiths, G. A. C. Jones, I. Farrer, and D. A. Ritchie, *Phys. Rev. Lett.* **106**, 126801 (2011).
- <sup>45</sup>M. W. Keller, N. M. Zimmerman, and A. L. Eichenberger, *Metrologia* **44**, 505 (2007).
- <sup>46</sup>J. D. Fletcher, M. Kataoka, S. P. Giblin, S. Park, H.-S. Sim, P. See, D. A. Ritchie, J. P. Griffiths, G. A. C. Jones, H. E. Beere, and T. J. B. M. Janssen, *Phys. Rev. B* **86**, 155311 (2012).
- <sup>47</sup>L. Devoille, N. Feltin, B. Steck, B. Chenaud, S. Sassine, S. Djordjevic, O. Séron, and F. Piquemal, *Meas. Sci. Technol.* **23**, 124011 (2012).
- <sup>48</sup>S. P. Giblin, P. See, A. Petrie, T. J. B. M. Janssen, I. Farrer, J. P. Griffiths, G. A. C. Jones, D. A. Ritchie, and M. Kataoka, *Appl. Phys. Lett.* **108**, 023502 (2016).